

Stress relaxation and creep response simulation of P92 steam piping under different loading conditions

S Salifu,¹ D Desai,¹ S Kok,² O Ogunbiyi,¹ A Oketola,¹ I Cipriano³

¹ Department of Mechanical and Mechatronics Engineering, Tshwane University of Technology, South Africa

² Department of Mechanical and Aeronautical Engineering, University of Pretoria, South Africa

³ Department of Industrial Engineering, Tshwane University of Technology, South Africa

Corresponding author: S Salifu **E-mail:** smithsalifu@gmail.com

In a quest to drastically reduce the cost of production of electrical energy and the dire need to meet the increasing demand for electricity, power generation steam pipings are exposed to different steam loading conditions. The different daily loading conditions/cycles are known to impact the creep behaviour and the pattern of stress relaxation in the steam piping. The creep response and stress relaxation of P92 steam piping subjected to different loading conditions were simulated using a finite element (FE) technique. Abaqus CAE/2020 was used to estimate the creep behaviour and stress relaxation of the piping while fe-safe/Turbolife was used in the computation of the creep damage and useful life of the pipe. Comparing the different conditions of operation, faster or swifter stress relaxation and higher creep strain were observed in the piping subjected to steady-state in relation to the analyses encompassing cyclic loadings. The piping's useful creep life when subjected to cyclic loading is lower than that obtained when subjected to steady-state analysis. Thus, any form of cyclic loading of steam piping greatly reduces its useful creep life.

Keywords: piping, creep stress, stress relaxation, creep damage, creep strain, useful life

Simulasie van spanningsvermindering en kruiprespons by P92-stoompype onder verskillende ladingstoestande: In 'n strewing om die koste van die produksie van elektriese energie drasties te verminder en die dringende behoefte om in die toenemende vraag na elektrisiteit te voorsien, word kragopwekkingstoempype aan verskillende stoamladingstoestande blootgestel. Dit is bekend dat die verskillende daaglikse ladingstoestande/-siklusse 'n beduidende impak op die kruipgedrag en die patroon van spanningsvermindering in die stoompype het. Gevolglik is die kruiprespons en spanningsvermindering van P92-stoompype wat aan verskillende ladingstoestande onderwerp is, gesimuleer deur in hierdie studie van 'n eindige-elementtegniek (EE-tegniek) gebruik te maak. Abaqus CAE/2020 is gebruik om die kruipgedrag en spanningsvermindering van die pype te raam, terwyl fe-safe/Turbolife in die berekening van die kruipskade en nutsduur van die pype gebruik is. Deur die verskillende bedryfstoeistande te vergelyk, is vinniger spanningsvermindering en hoër kruipvervorming waargeneem in die pype wat aan 'n bestendige toestand onderwerp is in verhouding tot die ontledings wat sikliese ladings omvat het. Die pype se kruipnutsduur wanneer dit aan sikliese lading onderwerp word, is korter as wat verkry word uit analyses wanneer dit aan 'n bestendige toestand onderwerp word. Dus verminder enige vorm van sikliese lading van stoompype kruipnutsduur aansienlik.

Sleutelwoorde: stoompype, kruipvervorming, spanningsvermindering, kruipskade, kruipvervorming, nutsduur

Introduction

As a crucial component of power generation plants, steam pipes serve as a means of conveying steam from the boiler compartment to the turbines. By virtue of this, steam pipes are operated under harsh conditions characterised by high operating temperatures and pressures. Hence, steam pipes must be fabricated from materials capable of withstanding these harsh service conditions (Salifu, et al., 2021a).

It was observed that the remaining life of power generation plants is greatly reduced when they are subjected to frequent start-up and shutdown cycles at high temperatures, as different damage processes such as softening resulting from cyclic loading, creep damage accumulation emanating from the holding period, and possible interactions between two failure modes, creep and fatigue (Wang, et al., 2018; Wang, et al., 2019; Song, et al., 2021) affect the remaining life of the steam pipes. Good knowledge of the creep behaviour of components, when subjected to different loading conditions, is essential, as it assists in the evaluation of the useful remaining life of power plant components such as steam pipes (Hyde, et al., 2010; Laha, et al., 2001; Tu, 2022).

The creep deformation and behaviour of P91 martensitic stainless steel at different temperatures have received a lot of attention in the research world in recent times (Eggelar, et al., 1994; Hyde, et al., 2006; Hyde, et al., 2010; Saber, et al., 2011), but little attention

has been paid to the new generation creep strength-enhanced ferritic stainless steel, P92, particularly when used as steam piping and subjected to different operating cycles (Sugiura, et al., 2010; Vaillant, et al., 2008). P92 with 9-12% chromium is one of the new generations of high creep strength-enhanced ferritic stainless steel that has found application in the power generation plants (both in nuclear and fossil-fuel plants) as super header components, steam pipes and other components that are used in high-temperature applications (Susmel & Taylor, 2003). Being a material with an improved creep strength at high temperatures, P92 allows the operation of critical and supercritical power stations where the operating temperature and pressure are much higher than that obtained in a conventional power plant (Saber, et al., 2011). Based on the higher operating temperature and pressure that P92 steam piping can withstand, it is paramount to have a good knowledge of the creep behaviour of the piping when subjected to different daily operating cycles during service.

Studies conducted on steam piping characterised by a combination of straight sections and elbows, and subjected to high-temperature operations showed that the optimum stress and strain developed due to creep are usually located at the elbows or bends (Salifu, et al., 2020a; Salifu, et al., 2020b). These regions are therefore more prone to failure, as they display a limiting creep life compared to the other regions (Salifu, et al., 2021a). The rapid accumulation of creep deformation in this region of the piping is the main mechanism for the failure experienced in steam piping (Lan, et al., 2018).

Over time, different estimation techniques have been employed to predict the creep behaviour of components with different shapes and sizes. Some of the frequently used methods are experimental, theoretical, and FE techniques. Experimental/theoretical techniques have been utilised successfully by different researchers in the estimation of the creep behaviour of components with simple geometric and boundary conditions (Lan, et al., 2018). Finite element techniques on the other hand are used for components having complex shapes and boundary conditions (Hyde, et al., 2002a; Hyde, et al., 2002b).

Being a commonly used technique for the determination of creep behaviour of components with complex shapes and boundary conditions, T.H. Hyde, et al., (2002a; 2002b) simulated the creep behaviour of an internally pressured 90-degree elbow pipe with ovality and without ovality. The creep life of the elbow pipe was observed to decrease as the damage position changed in the elbow's cross-section due to ovality. In a different study, J.P. Rouse, et al., (2013) numerically simulated the creep behaviour/response of a 90-degree elbow pipe by gradually varying its wall thickness. According to the study, it was observed that the stress redistribution in the elbow pipe is greatly affected by the disparity in the pipe's cross-sectional dimension, and this greatly influences the creep life of the pipe, particularly at the elbow.

To compute the creep behaviour of high creep strength-enhanced ferritic stainless steel, P92 steam piping, subjected

to different operating cycles in this study, the finite element (FE) technique was employed. The creep behaviour of the piping due to the different operating conditions was computed using FEA software, Abaqus CAE/2020, while the estimation/prediction of the damage due to creep and useful life of the piping were achieved using fe-safe/Turbolife, a post-processing software.

Developed stress in thick-walled pipe

Straight pipe whose ratio of inner diameter, D to the thickness, t is less than 20 is categorised as thick-walled pipe or cylinder, and these pipes are often used in power generation for conveying steam from the boiler compartments to the turbine. When steam flows through the pipe, thermo-mechanical stress is developed. During operation, the mechanical stress developed in the straight pipe can be estimated using Lamé's theory while the thermal stress equations for a thick-walled cylinder are used to calculate the developed thermal stress in the straight pipe. Using these two expressions, the developed thermo-mechanical stress in a thick-walled straight cylinder or pipe can be calculated (Kandil, et al., 1995; Pesonen, 2014).

Based on Lamé's theory (Kanlikama, et al., 2013), the equation for the hoop, longitudinal and radial mechanical stress developed when a thick pipe or cylinder is acted upon by an internal steam pressure P are given as:

$$\sigma_r = P \frac{r_i^2(r^2 - r_o^2)}{r^2(r_o^2 - r_i^2)} \quad (1)$$

$$\sigma_t = P \frac{r_i^2(r^2 + r_o^2)}{r^2(r_o^2 - r_i^2)} \quad (2)$$

$$\sigma_z = \frac{Pr_i^2}{r_o^2 - r_i^2} \quad (3)$$

Using the von-Mises theory (Equation (4)), the pipe's total/effective mechanical stress can be calculated.

$$\sigma_{vm} = \sqrt{[\sigma_t^2 + \sigma_r^2 + \sigma_z^2 - (\sigma_t\sigma_r + \sigma_t\sigma_z + \sigma_r\sigma_z)]} \quad (4)$$

where P represents the steam pressure applied, σ_r represents the induced radial mechanical stress, σ_t represents the developed circumferential mechanical stress, σ_z represents the induced axial mechanical stress and represents the effective mechanical Von-Mises stress.

For a straight and thick pipe at elevated temperatures, the developed thermal stress is calculated using the following expressions (Kandil, et al., 1995; Pesonen, 2014):

$$\sigma_{tT} = \frac{\alpha E}{(1-\nu)r^2} \left[\frac{r^2 + r_i^2}{r_o^2 - r_i^2} \int_{r_i}^{r_o} T r dr - \int_{r_i}^r T r dr - T r^2 \right] \quad (5)$$

$$\sigma_{rT} = \frac{\alpha E}{(1-\nu)r^2} \left[\frac{r^2 - r_i^2}{r_o^2 - r_i^2} \int_{r_i}^{r_o} T r dr - \int_{r_i}^r T r dr \right] \quad (6)$$

$$\sigma_{zT} = \frac{\alpha E}{(1-\nu)} \left[\frac{2}{r_o^2 - r_i^2} \int_{r_i}^{r_o} T r dr - T \right] \quad (7)$$

Thereafter, the von-Mises expression shown in Equation (8) is employed to calculate the developed effective thermal stress.

$$\sigma_{vmT} = \sqrt{[\sigma_{tT}^2 + \sigma_{rT}^2 + \sigma_{zT}^2 - (\sigma_{tT}\sigma_{rT} + \sigma_{tT}\sigma_{zT} + \sigma_{rT}\sigma_{zT})]} \quad (8)$$

where σ_{rT} represents the developed thermal radial stress, σ_{tT} represents the developed thermal circumferential stress, σ_{zT} represents the developed thermal axial stress and σ_{vmT} represents the effective/total thermal Von-Mises stress developed.

Thereafter, the individual mechanical and thermal effective von-Mises stresses are summed up to determine the effective thermo-mechanical stress in the thick straight pipe during operation. The expression for the developed effective thermo-mechanical stress developed in a straight thick pipe is shown in Equation (9).

$$\sigma_{TM} = \sigma_{vm} + \sigma_{vmT} \quad (9)$$

Conventional Hyperbolic Sine Creep Model

For components subjected to cyclic loading in a high-temperature creep region or environment, it is paramount that the creep model to be used does not only account for the steady-state creep process but must be able to adequately account for the creep behaviour at the different stress ranges resulting from the cyclic loading. Since the steam pipe in this study is subjected to cyclic loading in a creep regimen, a conventional hyperbolic sine creep model known for its exceptional ability to efficiently capture high and low-stress ranges, and adequately account for the creep behaviour in the face of cyclic loading, similar to those developed in power generation components was adopted (Montes, et al., 2012), and the model’s mathematical expression is given as (Salifu, et al. 2020b; Strang & Greenwood, 1998):

$$\dot{\epsilon}^{cr} = A \times \sinh(\beta\sigma) \quad (10)$$

where β represents the material constant; A is Arrhenius functions of the temperature (T) in Kelvin, and it is given as

$$A = Ke^{-C/T} \quad (11)$$

where K and C represent creep material constants for the model.

Creep Damage

If a component subjected to high-temperature operation exhibits limiting creep life prior to failure in the presence of cyclic loading, it is important to determine the time for which the different loadings are applied, and the best approach to achieve this is via Robinson’s linear creep damage or time fracture rule (Robinson, 1952; Liu, et al., 2017; Seruga, et al., 2011). According to the rule, the accumulation of damage in a single step time is independent of the previously accumulated damage, and failure will occur when the sum of the individual damages due to creep equals 1. Since the steam pipe in this study is subjected to daily cyclic loading, the time fracture rule also known as Robinson’s linear creep damage rule is deemed fit to compute the creep damage accumulation, as the expression accounts for the different startup and shut down cycles, such that failure will occur in the pipe if the summation of the individual creep damages equals unity. The expression for the summation of the linear creep damage is given as:

$$D_c = \sum \frac{t_i(\sigma)}{T_r(\sigma)} \quad (12)$$

where D_c represents creep damage, T_r is creep life before failure or rupture, and t_i represents the duration of creep duration for a given stress value and temperature increment i .

FE Model

The creep response of P92 fabricated steam piping, when subjected to different operating conditions was simulated using Abaqus CAE/2020, and fe-safe/Turbolife (a postprocessing software). Several steps were involved in the analyses, and they were observed sequentially. At first, heat transfer analysis is conducted on the piping with respect to the different operating conditions, thereafter, the creep analysis is driven by applying the nodal temperature developed in the pipe in the predefined field. After which the .odb (output database) results obtained from the creep analyses are exported and used in fe-safe/Turbolife (Fameso, et al., 2021) to compute the damage experienced by the piping due to creep, and the corresponding useful life of the piping for the different operations considered.

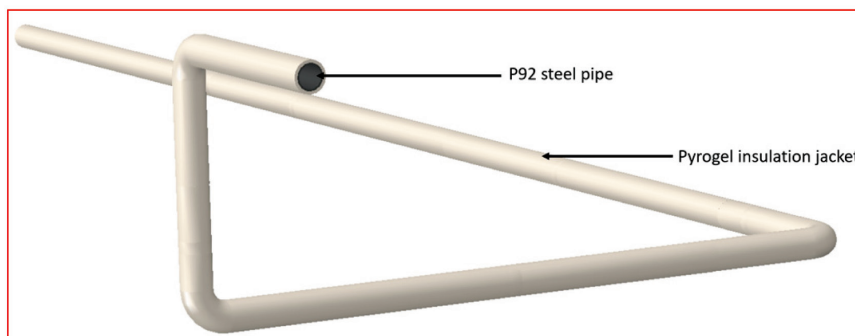


Figure 1: Assembly model of pipe-insulation jacket

Model Development

A model of the pipe-insulation jacket was created in Abaqus to replicate what is obtainable in a typical power generation plant. The assembly model of the piping is depicted in Figure 1 while the used dimensions for the piping and insulation jacket are shown in Table I.

The mechanical and thermal properties of P92 steel and the insulation jacket (pyrogel) employed in this study are depicted in Figure 2 and Table II, respectively while the constant for the used creep model (conventional hyperbolic sine creep model) for P92 steel used in this study (depicted in Table III) was obtained after curve fitting of existing P92 steel creep experimental data (Kral, et al., 2018).

Table I: P92 steam piping (Rasiawan, 2017; Salifu, et al., 2020a; Salifu, et al, 2020c), and pyrogel insulation jacket (Salifu, et al., 2020b; Salifu, et al., 2021c; Salifu, et al., 2021d) dimensions

Measurements	Dimension of P92-piping (m)	Dimension of pyrogel insulation jacket (m)
Total length	52,10	52,10
External diameter	0,44	0,54
Internal diameter	0,38	0,44
Thickness	0,03	0,05
Radius of elbow	0,50	0,50

During the steady-state analysis (heat transfer), an operating temperature of 550 with 10 000 W/m²K convective heat transfer coefficient was applied on the inner surface of the assembly while 25 with 18 W/m²K representing room temperature was applied on the exterior surface of the assembly (outer surface of the insulation jacket) (Salifu, et al., 2019; Salifu, et al., 2021b; Salifu, et al., 2021e; Ogunbiyi, et al., 2019). Also, an 18 MPa pressure load representing the operating pressure of steam was applied on the inner surface of the assembly. For the analyses consisting of different daily start-up and shutdown cycles, the operating temperatures and pressure used on the inner surface of the assembly are shown in Figures 3(a) and (b) while the description of the cycles is shown in Table IV. The outer temperature of the assembly is the same as that of the steady-state analysis regardless of the operational cycle considered.

Table III: Conventional hyperbolic creep model material constants for P92 steel

β ($\times 10^{-8}$ Pa)	C ($\times 10^4$ J)	K ($\times 10^{28}$)
6,3	7,2	2,0

Table II: Thermal/mechanical properties of insulation jacket (pyrogel) used (Salifu, et al, 2021d; Salifu, et al, 2021d; Pyrogel-XTE-Datasheet)

Elasticity [GPa]	Poisson Ratio	Expansion [$\times 10^{-6}$ K ⁻¹]	Density [kg/m ³]	Specific Heat Capacity [J/kgK]	Conductivity [$\times 10^{-3}$ W/mK]
10,0	0,20	4,0	170,0	2 300,0	64,0

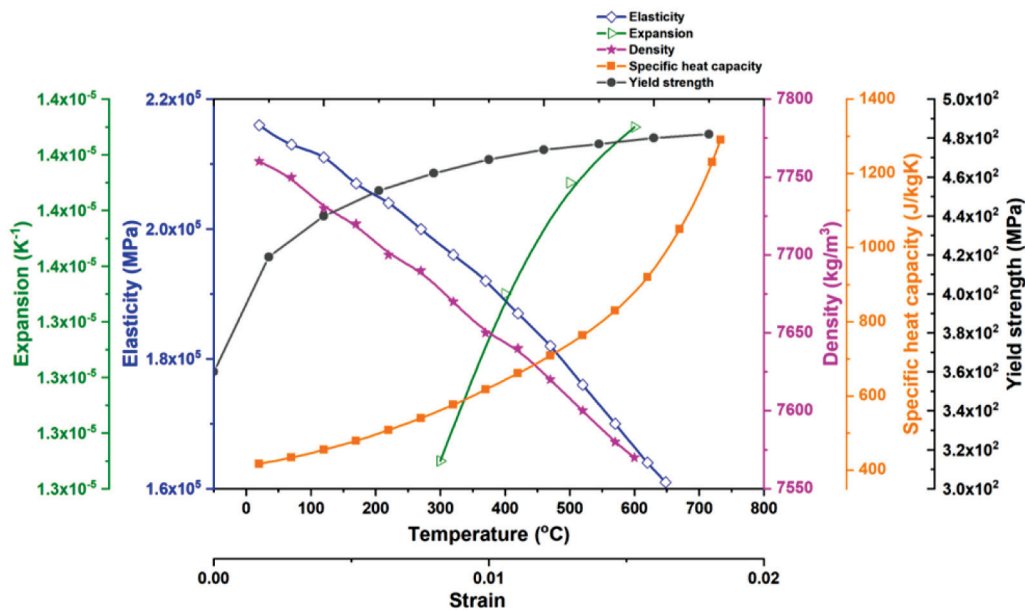


Figure 2: Thermal/mechanical properties of P92 steel (Salifu, et al., 2021a)

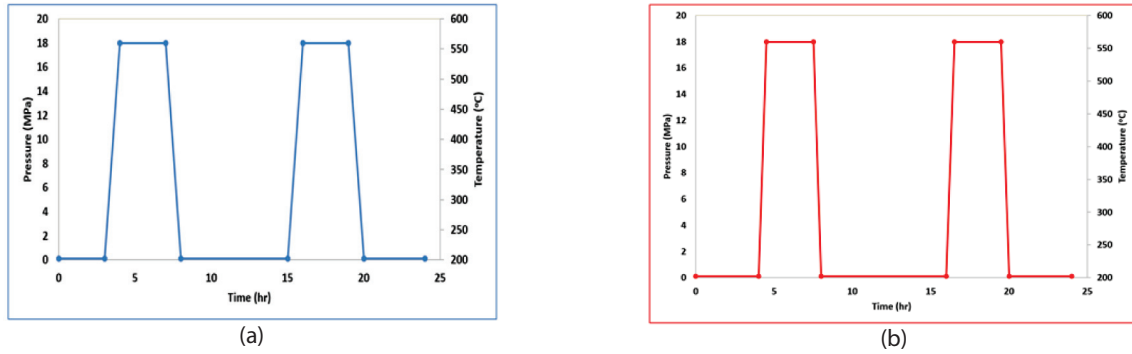


Figure 3: 24 hours operational (a) Cycle A1, and (b) Cycle A2

Table IV: Daily operational cycles description

Daily cycles		
Steady-state	Cycle A1	Cycle A2
Complete steady-state for 24 hours	A daily 24 hours cycle, having two 3 hours peaks, four 1-hour transient times, and 14 hours off-peak periods.	A daily 24 hours cycle, having two 3 hours peaks, four 30-minute transient times, and 16 hours off-peak periods.

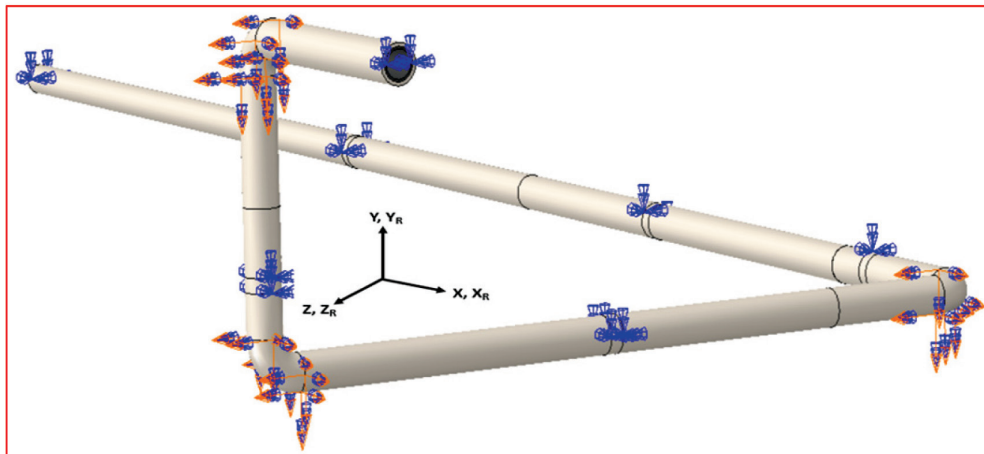


Figure 4: Applied boundary conditions on the assembly

Table V: Applied boundary conditions

Location on the piping network	Boundary conditions
Extreme ends	Displacement rotation X: Not fixed Y: Not fixed Z: Not fixed X_{R1} : Fixed Y_{R2} : Fixed Z_{R3} : Fixed
Elbows	Displacement rotation X: Not fixed Y: Not fixed Z: Not fixed X_{R1} : Not fixed Y_{R2} : Not fixed Z_{R3} : Not fixed
Supports	Displacement rotation X: Not fixed Y: Not fixed Z: Not fixed X_{R1} : Fixed Y_{R2} : Fixed Z_{R3} : Fixed

The mechanical boundary conditions assigned to the piping-insulation assembly mimic the real boundary condition applied to steam pipes in the power generation plants. Rotation/displacement boundary conditions that allow displacement of the assembly in the X, Y and Z; and elbow rotation in the direction X_{R1} , Y_{R2} and Z_{R3} as illustrated in Figure 4 were applied.

After the application of the appropriate mechanical boundary conditions and loading, an appropriate mesh size was applied to the assembly after conducting a convergence study by gradually reducing the size of the mesh until a result with high accuracy (above 90 %) is obtained at a moderate computational time. The outcome of the conducted convergence study is illustrated graphically in Figure 5 (a), and the assembly mesh illustrated in Figure 5(b), shows that a mesh size of 50 mm is appropriate for the analysis. 92 196 DC3D8 element types (“linear 8-node heat transfer brick”) were used in the heat transfer analysis while 92 196 C3D8R element types (“linear 8-node reduced integration, hourglass control brick”) were used in the creep analysis (Salifu, et al., 2021a).

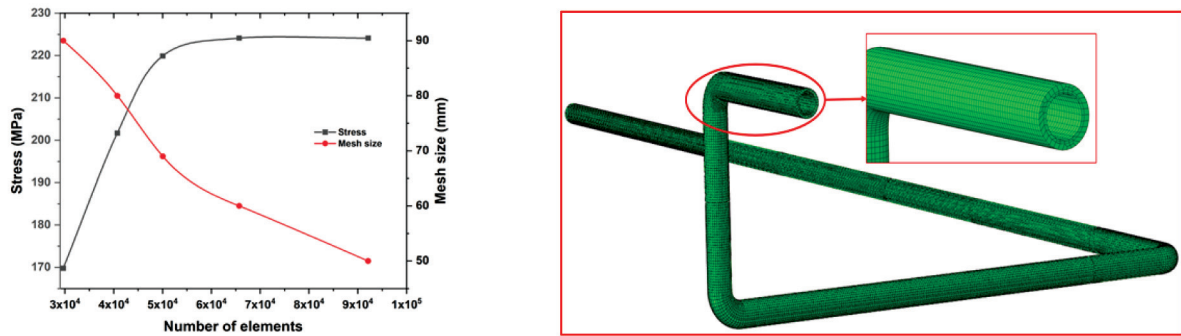


Figure 5: (a) Mesh convergence graph and (b) assembly mesh of pipe-insulation jacket

During the computation of the creep strain developed in the pipe for the different operating conditions considered, Abaqus first computes the thermo-mechanical stress developed in the piping due to the different operating pressure and temperature as specified in the different cycles the piping was subjected to. Thereafter, the value of the developed stress in conjunction with the creep material constants for the pipe then incorporated in the expression of the creep model used (conventional hyperbolic sine creep model) in the analysis. For the creep model, a user subroutine script was written in Fortran and implemented via a special user subroutine procedure. This is run in the background of the software during the analysis to produce the creep behaviour and the stress relaxation patterns for the operating cycles considered.

Creep Life

After conducting the creep analysis in Abaqus CAE/2020, the odb (output database) result obtained from the analysis (creep) was exported, and used in the post-processing software, fe-safeTurbolife to compute the piping creep damage, and the useful life for the different conditions considered. During the analyses, the piping was ascribed a machined-finish surface having surface roughness within $16 < Ra \leq 40 \mu\text{m}$ range and, Morrow stress correction was utilised in the analysis [39] in all the operating conditions considered.

Results and Discussion

The plot for temperature distribution across the thickness of the pipe-insulation assembly during a steady-state creep analysis is illustrated in Figure 6. It was obvious from the figure that the applied operation temperature, was conserved inside the piping as shown by the value of the maximum contour plot developed inside the piping. Also, the low-temperature value () obtained on the exterior surface of the assembly is a pointer to the fact that the piping is properly insulated and minimal heat loss occurs during operation. Hence, pyrogel can be classified in the category of suitable insulation for high-temperature components such as steam pipes.

Under the steady-state operation of the steam piping, the developed creep stress and strain developed after an hour of the analysis is depicted in Figure 7(a) and (b). From both figures, it was obvious that the optimum creep stress and strain in the piping is located at the intrados, and it was observed that the creep stress and strain decrease as steam flows away from the piping's intrados. Thus, the highest creep stress (216.1 MPa) and strain value was located at the piping's intrados, making the intrados most prone to creep failure when compared to the other regions.

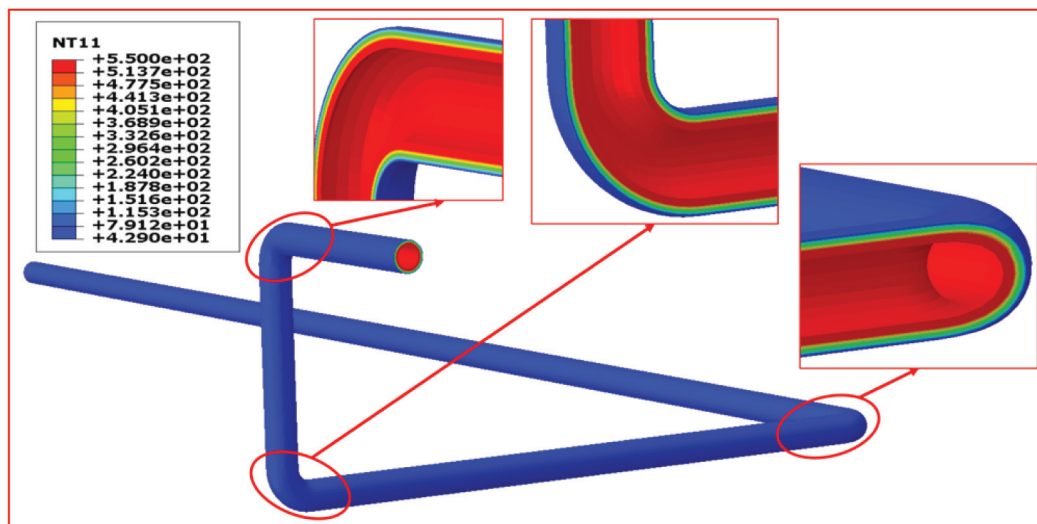


Figure 6: Steam piping temperature distribution profile in

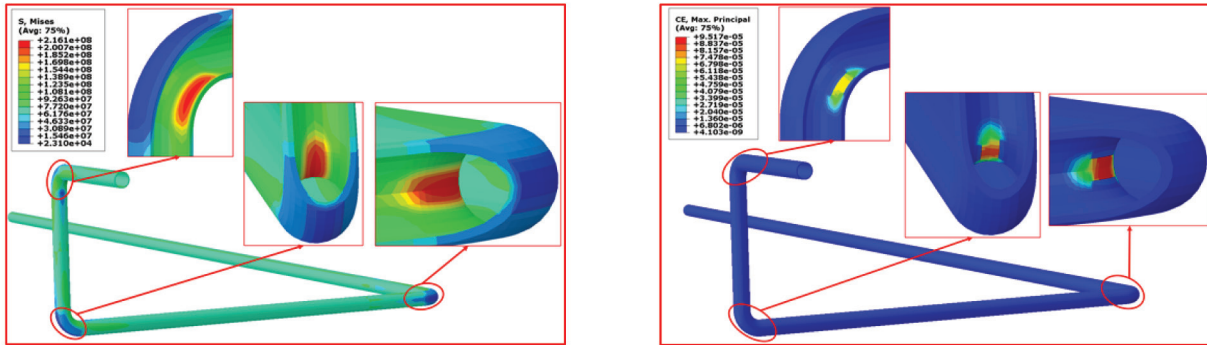


Figure 7: Steam piping creep (a) stress plot and (b) strain plot profile

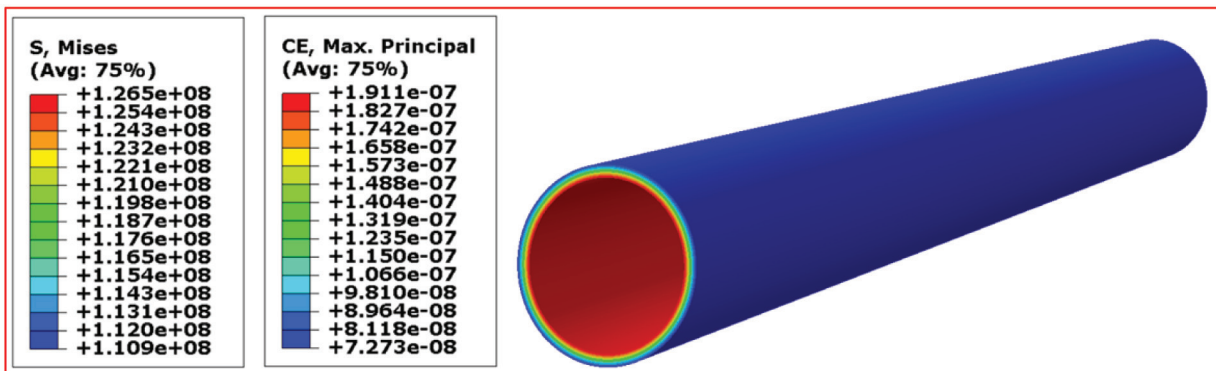


Figure 8: Developed creep stress and strain after one hour steady-state analysis in straight pipe

At a straight region far from the piping elbow and intrados, the developed stress and strain due to creep are lower than those developed at the intrados. Illustrated in Figure 8 is the profile of stress and strain due to creep developed in the straight section, at a location far away from the intrados, when the piping is subjected to steady-state analysis for one hour. Due to the simplicity of this region of the piping (straight pipe), the creep stress (126.5 MPa), and strain value is used for the analytical validation of the model.

The developed stress and strain contour plot due to creep at failure when the steam piping is operated at the three stated conditions is depicted in Figures 9 (a) and (b). Regardless of the operational condition, the piping was subjected to, the maximum stress and strain due to creep developed were located at the piping's intrados. Unlike in the analysis (steady-state) conducted for an hour, with results shown in Figure 8, the maximum stress and strain due to creep at failure are obvious and can be seen on the outer surface of the piping. At failure, the least stress (132.5 MPa) was obtained during steady-state analysis, while the analysis having a 30-minute transient time developed the highest stress (158.7 MPa). This behaviour is ascribed to the amount of time or the duration of the different analyses in the high-temperature creep environment, because the longer the time spent in the high-temperature environment, the faster the stress relaxation. Also, the relaxed stress value of the analysis involving one hour transient time is slightly lower than that with 30-minute transient time because it spent less time at off-peak as compared.

Unlike the pattern of the stress relaxation that decreases as the operation time increases, the creep strain increases with an increase in operational time, such that the highest creep strain was obtained in the steady-state analysis, while the least creep strain was obtained in the analysis with cycle 2A (30-minute transient time). The comparably low creep strain experienced in cycle 2A as compared to cycle 1A and the steady-state can be likened to the duration of each analysis in the high-temperature environment.

Depicted in Figure 10 is the creep damage accumulation for the cycles considered. From the graph, it is observed that the analysis with one-hour transient times (cycle A1) has the fastest accumulation of creep damage, followed by the analysis with 30-minute transient time (cycle A2), then the steady-state analysis. Based on this, it is clear that the operational cycle characterised by the start-up cycle and shutdown cycle is responsible for the rate of damage accumulation experienced in the piping. These patterns in turn influence the useful life of the piping.

The contour plot for creep damage and the useful life of the piping for the different cycles considered is depicted in Figure 11. Just like the stress and strain due to creep, the worse life was developed at piping intrados. However, the steady-state analysis has the highest useful creep life (21.27 years), while the analysis with one-hour transient times gave the lowest useful life (8.96 years). The discrepancy in the piping's useful life is attributed to the damage accumulation patterns during operation. Due

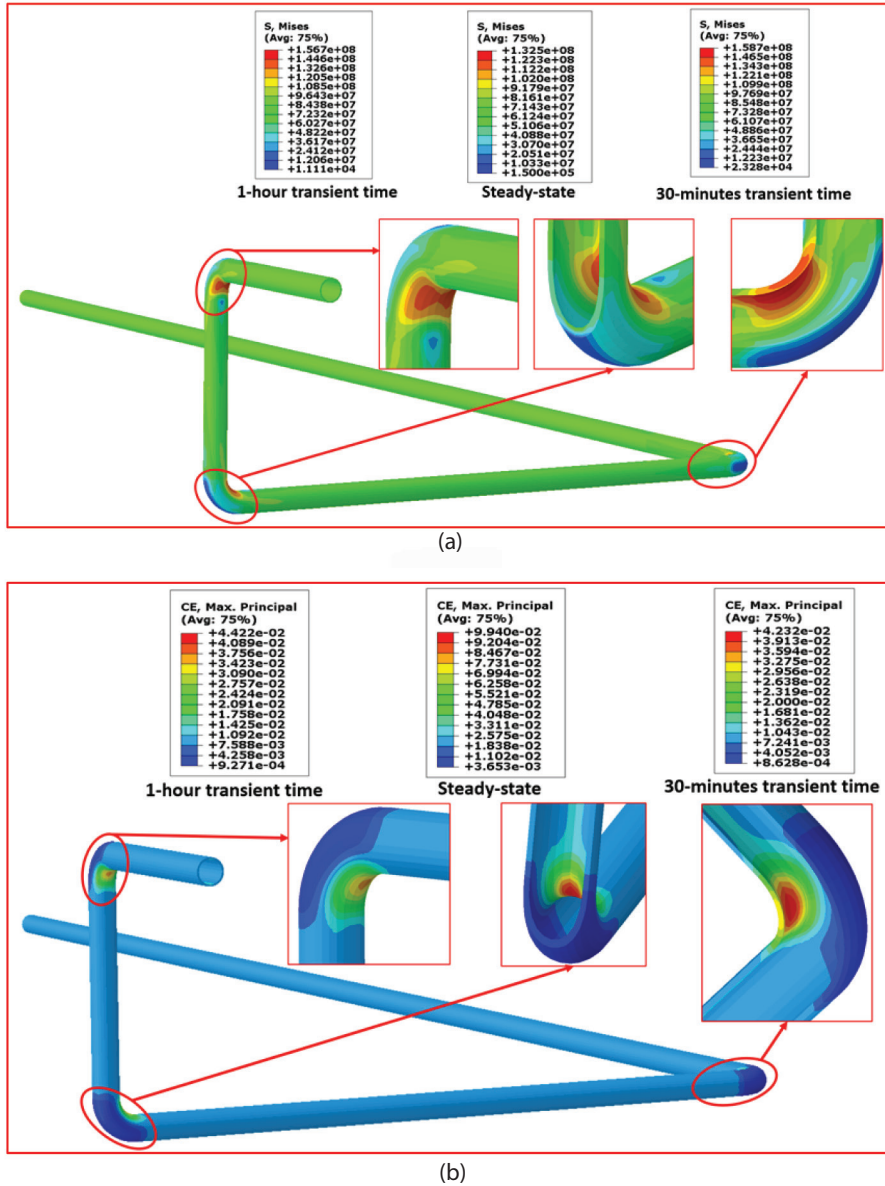


Figure 9: Creep (a) stress and (b) strain contour plot profile at failure

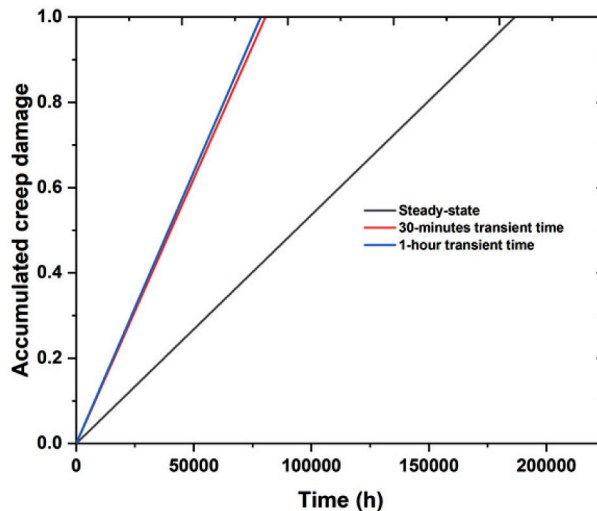


Figure 10: Creep damage accumulation of steam piping for the different cycles considered

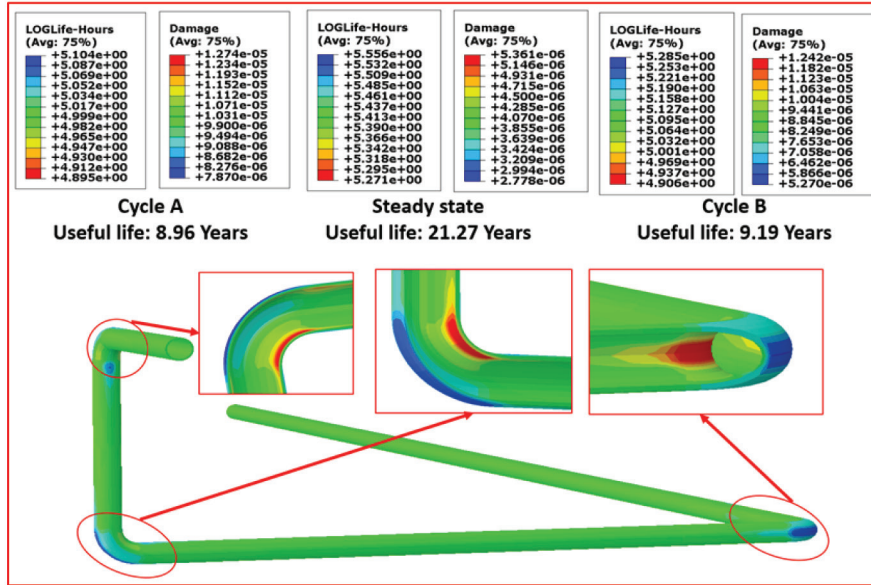


Figure 11: Steam piping creep damage and useful life at failure for operating cycles

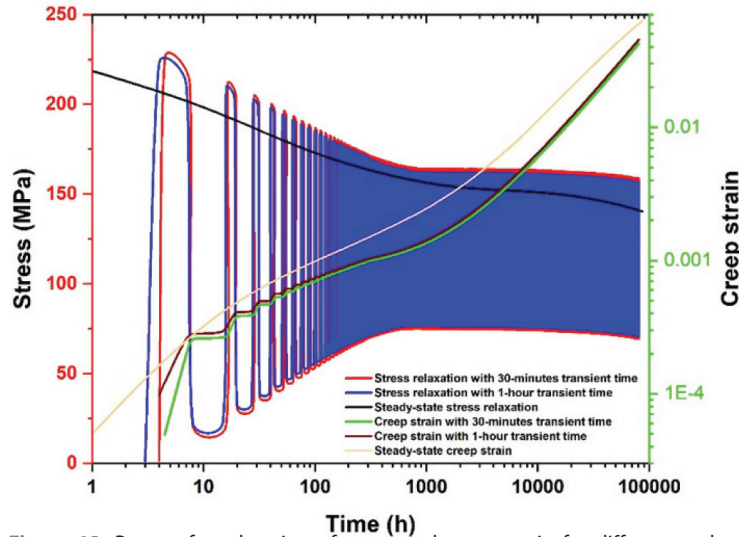


Figure 12: Pattern for relaxation of stress and creep strain for different cycles of operation

to the fast damage accumulation of the analysis with a one-hour transient time (cycle 1), it has the lowest useful creep life while the steady-state analysis with the slowest creep damage accumulation gave the highest useful creep life.

A plot of the stress pattern of the steam piping, for the different cycles considered, is illustrated in Figure 12. Since the entire operation time is spent in the high-temperature environment during the steady-state analysis, its stress relaxation is faster as compared to the two other analyses where only a fraction of their entire duration is spent in the high-temperature creep environment. Also, the stress relaxation of the analysis with one-hour transient times (cycle 1A) is faster than that with 30-minute transient times (cycle 2) because the analysis with 30-minute transient time (cycle 2) spent a longer time at off-peak as compared to that with one-hour transient time (cycle 1).

Furthermore, the creep strain at every time increment is observed to be higher in the steady-state analysis as compared to those with cycles. The reason for this behaviour is ascribed to the duration of each analysis in the high-temperature creep environment. Since the analysis with one-hour transient time spent lesser time at off-peak, its creep strain is slightly higher than that with 30-minute transient time.

Validation of creep strain

To validate the developed creep strain in the piping analytically, it is imperative to have an expression capable of computing the developed stress during operation. Nevertheless, the complexity of the piping, characterised by the presence of elbows makes the creep strain validation in the entire piping virtually impossible. However, the use of Lamé's equation for computing the mechanical stress (Equation 1-5), and the

equations for thermal stress determination (Equation 6-8) developed in a straight, thick-walled pipe, and the expression of the creep model (Equation 10) used in this study allows for the analytical validation of the developed creep strain at the straight section of the piping after one-hour of steady-state operation. The value of creep strain at the straight section of the piping after an hour of steady-state creep analysis obtained through FEA (shown in Figure 8), and that computed analytically using Equations 1-10 is depicted in Table VI. The comparison of both results using their percentage deviation shows that there is a strong correlation between the FEA and computed creep strain in the straight section of the steam piping.

Table VI: Comparison of FEA and analytically computed creep strain at the piping straight section

Creep strain		% deviation
FEA ($\times 10^{-7}$)	Analytically computed ($\times 10^{-7}$)	
1,911	1,951	2,05

Conclusion

In this study, finite element analysis software, Abaqus in conjunction with fe-safe/Turbolife post-processing software was used to determine the creep behaviour of P92 martensitic stainless steel steam piping subjected to different operating conditions often experienced in the electrical energy generation industries. Hence, the following deductions were made from the analysis:

- The applied operating temperature was retained inside the piping and the developed temperature value on the insulation jacket is a pointer that pyrogel is suitable for use as insulation for high-temperature equipment such as steam piping. Also, the outer temperature of the insulation jacket can further be reduced by increasing the jacket's thickness.
- The maximum creep stress and strain developed were located at the intrados of the piping in the different analyses considered, and this stress and strain becomes obvious at failure as indicated by the contour plots. Thus, the intrados is the most susceptible to failure in the entire piping assembly.
- A relatively fast relaxation in the stress with a corresponding higher creep strain was experienced in the steady-state creep analysis as compared to the analysis characterised by daily operational shifts. The reason for this behaviour was ascribed to the different duration of the piping in the high-temperature creep environment.
- The operation pattern rather than the creep strain is responsible for the rate of creep damage accumulation. Thus, the faster accumulation of creep damage during the daily cyclic loading.
- Due to the characteristic fast accumulation of creep damage suffered by the analysis with daily cyclic

loading, the piping subjected to steady-state operation gave the highest useful creep life.

- A strong correlation was obtained between the FEA creep strain and that computed analytically.
- Lastly, any form of daily cyclic loading results in faster damage accumulation which in return significantly reduces the creep life of the piping. Hence, steady-state remains the most ideal operating condition for steam pipes.

Acknowledgements

This research has been supported by Tshwane University of Technology and the University of Pretoria, South Africa. Also, the authors greatly appreciate the support of Eskom Power Plant Engineering Institute (Republic of South Africa).

Dates

Received: 19/06/2022
Accepted: 06/09/2022
Published: 26/10/2022

References

- Dassault-Systemes, 2017, fe-safe/TURBOLife user manual, *Dassault Systems, Providence, RI*, 122.
- Eggeler, G., Ramteke, A., Coleman, M., et al., 1994, Analysis of creep in a welded 'P91' pressure vessel, *International Journal of Pressure Vessels and Piping* 60(3), 237-257. [https://doi.org/10.1016/0308-0161\(94\)90125-2](https://doi.org/10.1016/0308-0161(94)90125-2).
- Fameso, F., Ramakokovhu, U., Desai, D., et al., 2021, Effects of manufacturing-induced operating-conditions amplified stresses on fatigue-life prediction of micro gas turbine blades-A simulation-based Study, *Journal of Physics: Conference Series* 2224, 012043. <https://doi.org/10.1088/1742-6596/2224/1/012043>.
- Hyde, T.H., Sun, W., Williams, J.A., 2002a, Life estimation of pressurised pipe bends using steady-state creep reference rupture stresses, *International Journal of Pressure Vessels and Piping* 79(12), 799-805. [https://doi.org/10.1016/S0308-0161\(02\)00134-5](https://doi.org/10.1016/S0308-0161(02)00134-5).
- Hyde, T.H., Yaghi, A., Becker, A.A., et al., 2002b, Finite element creep continuum damage mechanics analysis of pressurised pipe bends with ovality, *JSM International Journal Series A Solid Mechanics and Material Engineering* 45(1), 84-89. <https://doi.org/10.1299/jsmea.45.84>.
- Hyde, T.H., Becker, A.A., Sun, W., et al., 2006, Finite-element creep damage analyses of P91 pipes, *International Journal of Pressure Vessels and Piping* 83(11-12), 853-863. <https://doi.org/10.1016/j.ijpvp.2006.08.013>.
- Hyde, T.H., Saber, M., Sun, W., 2010, Testing and modelling of creep crack growth in compact tension specimens from a P91 weld at 650 °C, *Engineering Fracture Mechanics* 77(15), 2946-2957. <https://doi.org/10.1016/j.engfracmech.2010.03.043>.
- Kandil, A., El-Kady, A., El-Kafrawy, A., 1995, Transient thermal stress analysis of thick-walled cylinders, *International Journal of Mechanical Sciences*, 37(7), 721-732. [https://doi.org/10.1016/0020-7403\(94\)00105-5](https://doi.org/10.1016/0020-7403(94)00105-5).
- Kanlikama, B., Abuşoğlu, A., Güzelbey, İ.H., 2013, Coupled thermoelastic analysis of thick-walled pressurized cylinders, *International Journal of Energy and Power Engineering* 2(2), 60-68. <https://doi.org/10.11648/j.ijpe.20130202.15>.
- Kral, P., Dvorak, J., Sklenicka, V., et al., 2018, The effect of ultrafine-grained microstructure on creep behaviour of 9% Cr steel, *Materials* 11(5), 787. <https://doi.org/10.3390/ma11050787>.
- Laha, K., Chandravathi, K.S., Rao K.B.S., et al., 2001, An assessment of creep deformation and fracture behavior of 2.25 Cr-1Mo similar and dissimilar weld joints, *Metallurgical and Materials Transactions A* 32(1), 115-124. <https://doi.org/10.1007/s11661-001-0107-9>.
- Lan, X., Xu, H., Yang, L., et al., 2018, Influence of initial ovality on creep life of P92 pipe bends subjected to in-plane bending, *Materials at High Temperatures* 35(5), 418-426. <https://doi.org/10.1080/09603409.2017.1367156>.
- Liu, D., Pons, D.J., Wong, E.H., 2017, Creep-integrated fatigue equation for metals, *International Journal of Fatigue* 98, 167-175. <https://doi.org/10.1016/j.ijfatigue.2016.11.030>.

- Montes, J.M., Cuevas, F.G., Cintas, J., 2012, New creep law, *Materials Science and Technology* 28(3), 377-379. <https://doi.org/10.1179/1743284711Y.0000000029>.
- Ogunbiyi, O.F., Salifu, S.A., Jamiru, T., et al., 2019, Thermo-mechanical simulation of steam turbine blade with spark plasma sintering fabricated Inconel 738LC superalloy properties, *IOP Conference Series: Materials Science and Engineering* 655, 012046. <https://doi.org/10.1088/1757-899X/655/1/012046>.
- Pesonen, V., 2014, Online Creep and Fatigue Monitoring in Power Plants, *Master's Dissertation, Tampere University of Technology*.
- Pyrogel-XTE-Datasheet. High-performance aerogel insulation for industrial and commercial applications. Available: https://www.aerogel.com/_resources/common/userfiles/file/Data%20Sheets/Pyrogel-XTE-Datasheet.pdf.
- Rasiawan, T., 2017, The influence of prior creep damage on the fracture localisation in X20 CrMoV12-1 cross-weld creep tests, *Master's Dissertation, University of Cape Town*.
- Robinson, E.L., 1952, Effect of temperature variation on the long-time rupture strength of steels, *Journal of Fluids Engineering* 77, 777-780. <https://doi.org/10.1115/1.4015916>.
- Rouse, J.P., Leom, M.Z., Sun, W., et al., 2013, Steady-state creep peak rupture stresses in 90° powerplant pipe bends with manufacture induced cross-section dimension variations, *International Journal of Pressure Vessels and Piping* 105, 1-11. <https://doi.org/10.1016/j.ijpvp.2013.02.002>.
- Saber, M., Tanner, D.W.J., Sun, W., et al., 2011, Determination of creep and damage properties for P92 at 675 C, *The Journal of Strain Analysis for Engineering Design* 46(8), 842-851. <https://doi.org/10.1177/0309324711413012>
- Salifu, S., Desai, D., Kok, S., et al., 2019, Thermo-mechanical stress simulation of unconstrained region of straight X20 steam pipe, *Procedia Manufacturing* 35, 1330-1336. <https://doi.org/10.1016/j.promfg.2019.05.021>
- Salifu, S., Desai, D., Kok, S., 2020a, Comparative evaluation of creep response of X20 and P91 steam piping networks in operation, *The International Journal of Advanced Manufacturing Technology* 109(7), 1987-1996. <https://doi.org/10.1007/s00170-020-05727-7>.
- Salifu, S., Desai, D., Kok, S., 2020b, Prediction and comparison of creep behavior of X20 steam plant piping network with different phenomenological creep models, *Journal of Materials Engineering and Performance* 29, 7382-7395. <https://doi.org/10.1007/s11665-020-05235-5>.
- Salifu, S., Desai, D., Kok, S., 2020c, Creep-fatigue interaction of P91 steam piping subjected to typical start-up and shutdown cycles, *Journal of Failure Analysis and Prevention* 20, 1055-1064. <https://doi.org/10.1007/s11668-020-00908-8>.
- Salifu, S., Desai, D., Kok, S., 2021a, Influence of diverse operating cycles on the useful creep life of P92 steam piping, *Journal of Failure Analysis and Prevention* 21, 983-992. <https://doi.org/10.1007/s11668-021-01144-4>.
- Salifu, S., Desai, D., Fameso, F., et al., 2021b, Thermo-mechanical analysis of bolted X20 steam pipe-flange assembly, *Materials Today: Proceedings* 38(2), 842-849. <https://doi.org/10.1016/j.matpr.2020.04.882>
- Salifu, S., Desai, D., Kok, S., 2021c, Numerical simulation and creep-life prediction of X20 steam piping, *Materials Today: Proceedings* 38(2), 893-898. <https://doi.org/10.1016/j.matpr.2020.05.125>
- Salifu, S., Desai, D., Kok, S., 2021d, Numerical investigation of creep-fatigue interaction of straight P91 steam pipe subjected to start-up and shutdown cycles, *Materials Today: Proceedings* 38(2), 1018-1023. <https://doi.org/10.1016/j.matpr.2020.05.613>.
- Salifu, S., Desai, D., Kok, S., 2021e, Numerical simulation of stress relaxation and creep response of X20 steam piping under diverse operating conditions, *International Journal of Engineering Research in Africa* 57, 19-32. <https://doi.org/10.4028/www.scientific.net/JERA.57.19>.
- Šeruga, D., Fajdiga, M., Nagode, M., 2011, Creep damage calculation for thermo mechanical fatigue, *Strojniški vestnik-Journal of Mechanical Engineering* 57(5), 371-378. <https://doi.org/10.5545/sv-jme.2010.108>.
- Song, Y., Ma, Y., Chen, H., et al., 2021, The effects of tensile and compressive dwells on creep-fatigue behavior and fracture mechanism in welded joint of P92 steel, *Materials Science and Engineering: A* 813(5), 141129. <https://doi.org/10.1016/j.msea.2021.141129>.
- Strang, A., Greenwood, G.W., 1998, Microstructural stability of creep resistant alloys for high temperature plant applications. *IOM Communications (London)*, 1998.
- Sugura, R., Yokobori Jr, A.T., Suzuki, K., et al., 2010, Characterization of incubation time on creep crack growth for weldments of P92, *Engineering Fracture Mechanics* 77(15), 3053-3065. <https://doi.org/10.1016/j.engfracmech.2010.04.025>.
- Susmel, L. and Taylor, D., 2003, Two methods for predicting the multiaxial fatigue limits of sharp notches, *Fatigue & Fracture of Engineering Materials & Structures* 26(9), 821-833. <https://doi.org/10.1046/j.1460-2695.2003.00683.x>
- Tu, S.T., 2002, Creep behavior of crack near bi-material interface characterized by integral parameters, *Theoretical and Applied Fracture Mechanics* 38(2), 203-209. [https://doi.org/10.1016/S0167-8442\(02\)00088-5](https://doi.org/10.1016/S0167-8442(02)00088-5).
- Vaillant, J.C., Vandenberghe, B., Hahn, B., et al., 2008, T/P23, 24, 911 and 92: New grades for advanced coal-fired power plants-Properties and experience, *International Journal of Pressure Vessels and Piping* 85(1-2), 38-46. <https://doi.org/10.1016/j.ijpvp.2007.06.011>.
- Wang, X., Zhang, W., Gong, J., et al., 2018, Low cycle fatigue and creep fatigue interaction behavior of 9Cr-0.5 Mo-1.8 W-Nb heat-resistant steel at high temperature, *Journal of Nuclear Materials* 505, 73-84. <https://doi.org/10.1016/j.jnucmat.2018.03.055>.
- Wang, X., Zhang, W., Zhang, T., et al., 2019, A new empirical life prediction model for 9-12% Cr steels under low cycle fatigue and creep fatigue interaction loadings, *Metals* 9(2), 183. <https://doi.org/10.3390/met9020183>.